

# Spin identification of the mono- $Z'$ resonance in muon-pair production at the ILC with simulated electron-positron collisions at $\sqrt{s} = 500$ GeV

S. Elgammal\*

*Centre for Theoretical Physics, The British University in Egypt,  
P.O. Box 43, El Sherouk City, Cairo 11837, Egypt.*

(Dated: April 24, 2025)

In this analysis, we investigate the angular distribution of low-mass dimuon pairs produced in simulated electron-positron collisions at the proposed International Linear Collider (ILC), which operates at a center of mass energy of 500 GeV and an integrated luminosity of  $1000 \text{ fb}^{-1}$ . We focus on the  $\cos\theta_{\text{CS}}$  variable, defined in the Collins-Soper frame. In the Standard Model, the production of low-mass dimuon pairs is primarily driven by the Drell-Yan process, which exhibits a pronounced forward-backward asymmetry. However, many scenarios beyond the Standard Model predict different shapes for the  $\cos\theta_{\text{CS}}$  distribution. This angular distribution can be instrumental in distinguishing between these models in the event of excess observations beyond the Standard Model. We have used the mono- $Z'$  model to interpret the simulated data for our analysis. In the absence of any discoveries of new physics, we establish upper limits at the 95% confidence level on the masses of various particles in the model, including the spin-1  $Z'$  boson, as well as fermionic dark matter.

## I. INTRODUCTION

One potential method for detecting physics beyond the Standard Model (SM) of particle physics at future electron-positron colliders is to observe changes in the dilepton mass spectrum. These changes may manifest as a new peak, which is predicted by models involving neutral gauge bosons, such as  $Z'$  [1] or Randall-Sundrum [2], or as a broad distortion of the spectrum. Such distortions could suggest the presence of Contact Interactions [3, 4] or models like ADD [5]. To validate these theories, the mass spectrum should indicate an excess or deficit of events compared to the background prediction, primarily influenced by the Drell-Yan process.

The CMS collaboration has conducted a detailed study of signatures related to  $Z'$  and Contact Interaction models [6]. Both the ATLAS and CMS collaborations have previously searched for the massive extra neutral gauge boson  $Z'$ , which is predicted by Grand Unified Theory (GUT) and Supersymmetry [7–10]. However, there is currently no evidence after analyzing the entire RUN II period of LHC data [6, 11]. The results from the CMS experiment have excluded the existence of  $Z'$ , at a 95% Confidence Level (CL), for mass values ranging from 0.6 to 5.15 TeV, while the ATLAS experiment has ruled out mass values between 0.6 and 5.1 TeV.

The angular distributions of the leptons are also expected to be affected. Previous studies conducted by the CMS [12] and ATLAS [13] collaborations analyzed the angular distributions of Drell-Yan charged lepton pairs near the Z-boson mass peak to measure the forward-backward asymmetry, denoted as  $A_{FB}$ . Both studies utilized the complete LHC Run 1 dataset, which corresponds to an integrated luminosity of  $19.7 \text{ fb}^{-1}$  for CMS

and  $20.3 \text{ fb}^{-1}$  for ATLAS from proton-proton collisions at an 8 TeV center-of-mass energy ( $\sqrt{s}$ ). The results indicated that the measurements of  $A_{FB}$  are consistent with the predictions of the Standard Model. Furthermore, the forward-backward asymmetry of high-mass dilepton events (with invariant mass  $M_{ll} > 170 \text{ GeV}$ ) has been measured using the CMS detector at a center-of-mass energy of  $\sqrt{s} = 13 \text{ TeV}$ , with an integrated luminosity of  $138 \text{ fb}^{-1}$ . This analysis concluded that no statistically significant deviations from the predictions of the Standard Model have been observed [14].

Many dark matter (DM) searches have been conducted by analyzing data collected from the CMS and ATLAS experiments during RUN II [15, 16]. These searches focus on the production of a visible object, denoted as "X," which recoils against the substantial missing transverse energy resulting from dark matter particles. This creates a signature of  $(X + E_T^{\text{miss}})$  in the detector [17]. The visible particle "X" could be a Standard Model (SM) particle, such as W or Z bosons, jets [18–21], a photon [22, 23], or even the SM Higgs boson [24–26].

Additionally, the searches for dark matter in association with the Z boson [27, 28] and hard photons [29, 30] have been conducted at future electron-positron colliders such as the ILC [31] and CLIC [32].

Current collider experiments, including ATLAS and CMS, have established stringent limits on the coupling of the  $Z'$  particle to Standard Model (SM) leptons, denoted as  $g_l$ . Based on observations of four-muon final states, the coupling constant  $g_l$  is ruled out in the range of 0.004 to 0.3, depending on the mass of the  $Z'$  boson [33, 34].

Additionally, at high  $Z'$  masses (specifically for  $M_{Z'} > 200 \text{ GeV}$ ), the ATLAS collaboration has searched for dark matter [35] within the framework of the mono- $Z'$  model [36, 37], focusing on the leptonic decay channel of  $Z'$  at the LHC. This search has excluded  $Z'$  masses between 200 and 1000 GeV and has imposed specific constraints on  $g_l$ . Therefore, in the light-vector scenario,  $g_l$

\* sherif.elgammal@bue.edu.eg

is excluded in the range of 0.01–0.025 for lower  $Z'$  masses and 0.02–0.38 for higher  $Z'$  masses, specifically between 200 and 1000 GeV.

Previous collider experiments, like the LEP-2 [38], have shed light on important insights. For  $Z'$  masses exceeding the center-of-mass energy of  $\sqrt{s} = 209$  GeV, the LEP collaboration set a limit of  $g_l \leq 0.044 M_{Z'}/(200 \text{ GeV})$ . Conversely, for  $M_{Z'} < 209$  GeV, the limit on  $g_l$  remains at  $g_l \leq 0.044$  [39].

If the  $Z'$  does not couple to quarks, the HL-LHC and future hadron colliders will be unable to provide limits on its existence. In this case, electron-positron colliders like the proposed International Linear Collider (ILC) will be crucial. The ILC is set to operate at 500 GeV center of mass energy ( $\sqrt{s}$ ) initially, with an upgrade option to 1000 GeV [40–43]. Linear electron-positron colliders offer controllable energy, reduced QCD background, and adjustable beam polarization.

This analysis explores light neutral gauge bosons ( $Z'$ ) with a mass  $M_{Z'} \leq 100$  GeV, based on the light vector (LV) simplified model within the mono- $Z'$  framework [36]. We examine simulated electron-positron collisions at the ILC with 500 GeV center of mass energy, focusing on dimuon events from  $Z'$  decay and large missing transverse energy linked to dark matter.

This paper is structured as follows: Section II introduces the Collins-Soper frame and the  $\cos\theta_{CS}$  variable for Drell-Yan events. Section III presents the theoretical framework of the mono- $Z'$  portal model. In section IV, we discuss the simulation techniques for signal and SM background samples. Section V covers the selection cuts and analysis strategy. Finally, sections VI and VII present the results and summary of the analysis.

## II. THE COLLINS-SOPER FRAME

When an electron and positron collide, they can produce a lepton pair ( $l^+l^-$ ). The angle  $\theta$  measures the angle between the negative lepton and the incoming electron or positron in the center of the mass frame. The primary process for producing this pair at the tree level in the Standard Model is the Drell-Yan process ( $e^-e^+ \rightarrow \gamma^*/Z \rightarrow l^+l^-$ ). Our analysis focuses on the angular distribution of  $l^+l^-$  pairs in the Collins-Soper frame [44], which reduces distortions from the transverse momenta of the colliding particles. We use the Collins-Soper frame to analyze the angular distribution of lepton pairs, defining the angle  $\theta_{CS}$  as the angle between the negative lepton momentum and the z-axis.

To determine the Collins-Soper frame orientation, we use the sign of the longitudinal boost of the dilepton system. The angle  $\cos\theta_{CS}$  can be computed from measurable lab frame quantities, as explained in [12].

$$\cos\theta_{CS} = \frac{|Q_z|}{Q_z} \frac{2(P_1^+ P_2^- - P_1^- P_2^+)}{\sqrt{Q^2(Q^2 + Q_T^2)}}. \quad (1)$$

The symbols  $Q$ ,  $Q_T$ , and  $Q_z$  stand for the four-momentum, the transverse momentum, and the longitudinal momentum of the dilepton system, respectively. Similarly,  $P_1$  ( $P_2$ ) represents the four-momentum of  $l^-$  ( $l^+$ ), and  $E_i$  denotes the energy of the lepton. In addition,  $P_i^\pm$  is defined as  $(E_i \pm P_{z,i})/\sqrt{2}$ .

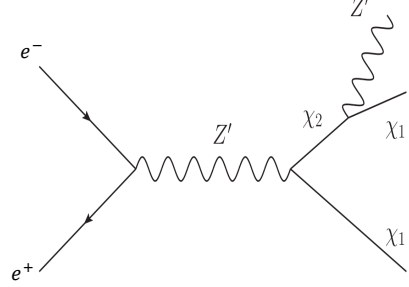


Figure 1 Feynman diagram for the Light Vector (LV) scenario based on mono- $Z'$  model; for the production of neutral light gauge boson ( $Z'$ ) in association to dark matter ( $\chi_1$ ) pair [36].

## III. THE SIMPLIFIED MODEL IN THE FRAMEWORK OF MONO- $Z'$ PORTAL

The mono- $Z'$  model discussed in [36] describes dark matter production from electron-positron collisions at the ILC via a new light gauge boson  $Z'$ . It includes two minimal renormalizable scenarios: the first involves dark-Higgsstrahlung from a  $Z'$  with invisible decay of the dark Higgs. In contrast, the second involves two states,  $\chi_{1,2}$ , coupling off-diagonally to the  $Z'$ . The  $Z' + E_T^{miss}$  search is more sensitive than direct resonance searches, especially for low  $Z'$  masses. This analysis focuses on the second light vector (LV) scenario, as shown in Figure 1.

The proposed dark matter is produced through electron-positron pair annihilation mediated by a light vector boson  $Z'$ . This process results in two types of dark matter: a light dark matter ( $\chi_1$ ) and a heavier one ( $\chi_2$ ), which decays to a  $Z'$  and  $\chi_1$  (i.e.  $\chi_2 \rightarrow Z' \chi_1$ ).

The interaction term, in the Lagrangian, between the dark fermions and  $Z'$  is given by [36]

$$\frac{g_{DM}}{2} Z'_\mu (\bar{\chi}_2 \gamma^\mu \gamma^5 \chi_1 + \bar{\chi}_1 \gamma^\mu \gamma^5 \chi_2),$$

where  $g_{DM}$  denotes the coupling of  $Z'$  to dark matter  $\chi_1$ . The coupling of  $Z'$  to visible leptons is represented by  $g_l$ .

In the LV scenario, the only permitted decay processes are as follows:  $Z' \rightarrow \chi_1 \chi_2$ ,  $\chi_2 \rightarrow Z' \chi_1$ , and  $Z' \rightarrow \mu^+ \mu^-$ . The total decay widths of both the  $Z'$  and  $\chi_2$  can be calculated using the masses of  $Z'$  and the dark matter, along with the relevant coupling constants. The free parameters in this scenario include the lightest dark matter

Scenario	Masses assumptions
Light dark sector	$M_{\chi_1} = 1, 5, \dots, 200 \text{ GeV}$
	$M_{\chi_2} = M_{\chi_1} + M_{Z'} + 25 \text{ GeV}$

Table I The Light mass assumptions for the dark sector for the light vector scenario [36].

mass  $M_{\chi_1}$ , the mass of the second dark matter particle  $M_{\chi_2}$ , the mass of the  $Z'$  boson ( $M_{Z'}$ ), and the couplings of  $Z'$  to both leptons and dark matter particles,  $g_l$  and  $g_{DM}$ , respectively.

The CMS and ATLAS detectors have extensively searched for  $Z'$  bosons over the years, confirming that heavy neutral gauge bosons do not exist in the mass range of 0.2 to 5.15 TeV. Therefore, we focus on the production of light neutral gauge bosons ( $Z'$ ) below 100 GeV at the ILC.

We consider the LV scenario using the light-dark sector model to provide mass to the dark matter particles ( $\chi_1$  and  $\chi_2$ ), as detailed in table I. This choice of  $M_{\chi_1}$  and  $M_{\chi_2}$  follows a prescription from [36], but it is just one possible option.

Due to previous restrictions from experiments like CMS, ATLAS, and LEP-2, the value of  $g_l$  is approximately 0.003 for  $M_{Z'}$  between 10 and 100 GeV [39]. In contrast,  $g_{DM}$  is set to 1.0 [36], while the masses ( $M_{Z'}$ ,  $M_{\chi_1}$ , and  $M_{\chi_2}$ ) are varied.

#### IV. SIMULATION OF SIGNAL SAMPLES AND SM BACKGROUNDS

The SM background processes yielding muon pairs in the signal region are Drell-Yan ( $DY \rightarrow \mu^+\mu^-$ ) production, the production of top quark pairs ( $t\bar{t} \rightarrow \mu^+\mu^- + 2b + 2\nu$ ) and production of diboson ( $W^+W^- \rightarrow \mu^+\mu^- + 2\nu$ ,  $ZZ \rightarrow \mu^+\mu^- + 2\nu$  and  $ZZ \rightarrow 4\mu$ ).

The LV scenario signal samples and corresponding SM background processes were generated using WHIZARD event generator 3.1.1 [45]. The ISR effect was included and interfaced with Pythia 6.24 for the parton shower model and hadronization [46]. For a fast detector simulation of the ILD detector, the DELPHES package [47] was used. These were generated from electron-positron collisions at the ILC with a 500 GeV center of mass energy, which corresponds to the circumstances of RUN I. The polarized degrees of electron and positron beams are  $P_{e^-} = 0.8$  and  $P_{e^+} = -0.3$ , respectively.

For the scenario where light vectors are produced along with dark matter particles ( $\chi_1$  and  $\chi_2$ ), we have considered the mass assumptions as summarized in Table I. Assuming  $g_l = 0.003$  and  $g_{DM} = 1.0$ , table II shows the production cross section times branching ratios at Leading Order (LO) for various mass points of  $Z'$  and DM.

$\frac{M_{Z'}}{M_{\chi_1}}$	10	20	30	40	50	60	70	80	90	100	150
1	$7.73 \times 10^{-1}$	$7.08 \times 10^{-1}$	$6.73 \times 10^{-1}$	$6.49 \times 10^{-1}$	$6.28 \times 10^{-1}$	$6.12 \times 10^{-1}$	$6.01 \times 10^{-1}$	$5.88 \times 10^{-1}$	$5.78 \times 10^{-1}$	$5.69 \times 10^{-1}$	$5.37 \times 10^{-1}$
5	$7.63 \times 10^{-1}$	$6.87 \times 10^{-1}$	$6.52 \times 10^{-1}$	$6.29 \times 10^{-1}$	$6.09 \times 10^{-1}$	$5.95 \times 10^{-1}$	$5.82 \times 10^{-1}$	$5.70 \times 10^{-1}$	$5.60 \times 10^{-1}$	$5.51 \times 10^{-1}$	$5.17 \times 10^{-1}$
10	$7.62 \times 10^{-1}$	$6.65 \times 10^{-1}$	$6.30 \times 10^{-1}$	$6.05 \times 10^{-1}$	$5.86 \times 10^{-1}$	$5.73 \times 10^{-1}$	$5.59 \times 10^{-1}$	$5.48 \times 10^{-1}$	$5.39 \times 10^{-1}$	$5.29 \times 10^{-1}$	$4.91 \times 10^{-1}$
25	$6.44 \times 10^{-1}$	$6.20 \times 10^{-1}$	$5.75 \times 10^{-1}$	$5.47 \times 10^{-1}$	$5.27 \times 10^{-1}$	$5.12 \times 10^{-1}$	$4.98 \times 10^{-1}$	$4.86 \times 10^{-1}$	$4.76 \times 10^{-1}$	$4.66 \times 10^{-1}$	$4.21 \times 10^{-1}$
70	$5.58 \times 10^{-1}$	$5.19 \times 10^{-1}$	$4.79 \times 10^{-1}$	$4.41 \times 10^{-1}$	$4.04 \times 10^{-1}$	$3.66 \times 10^{-1}$	$3.31 \times 10^{-1}$	$2.95 \times 10^{-1}$	$2.60 \times 10^{-1}$	$2.42 \times 10^{-1}$	$2.28 \times 10^{-1}$
100	$6.30 \times 10^{-1}$	$3.80 \times 10^{-1}$	$3.15 \times 10^{-1}$	$2.82 \times 10^{-1}$	$2.59 \times 10^{-1}$	$2.40 \times 10^{-1}$	$2.24 \times 10^{-1}$	$2.10 \times 10^{-1}$	$1.94 \times 10^{-1}$	$1.81 \times 10^{-1}$	$1.17 \times 10^{-1}$
125	$4.46 \times 10^{-1}$	$2.69 \times 10^{-1}$	$2.20 \times 10^{-1}$	$1.93 \times 10^{-1}$	$1.73 \times 10^{-1}$	$1.56 \times 10^{-1}$	$1.41 \times 10^{-1}$	$1.28 \times 10^{-1}$	$1.17 \times 10^{-1}$	$1.02 \times 10^{-1}$	$4.64 \times 10^{-2}$
130	$4.08 \times 10^{-1}$	$2.47 \times 10^{-1}$	$2.01 \times 10^{-1}$	$1.76 \times 10^{-1}$	$1.56 \times 10^{-1}$	$1.40 \times 10^{-1}$	$1.26 \times 10^{-1}$	$1.12 \times 10^{-1}$	$1.00 \times 10^{-1}$	$8.77 \times 10^{-2}$	$3.53 \times 10^{-2}$
145	$2.96 \times 10^{-1}$	$1.82 \times 10^{-1}$	$1.47 \times 10^{-1}$	$1.26 \times 10^{-1}$	$1.10 \times 10^{-1}$	$9.60 \times 10^{-2}$	$8.34 \times 10^{-2}$	$7.18 \times 10^{-2}$	$6.07 \times 10^{-2}$	$5.05 \times 10^{-2}$	$1.10 \times 10^{-2}$
170	$1.35 \times 10^{-1}$	$8.95 \times 10^{-2}$	$7.07 \times 10^{-2}$	$5.77 \times 10^{-2}$	$4.67 \times 10^{-2}$	$3.72 \times 10^{-2}$	$2.86 \times 10^{-2}$	$2.12 \times 10^{-2}$	$1.48 \times 10^{-2}$	$9.46 \times 10^{-3}$	$8.39 \times 10^{-6}$
175	$1.10 \times 10^{-1}$	$7.41 \times 10^{-2}$	$5.81 \times 10^{-2}$	$4.64 \times 10^{-2}$	$3.68 \times 10^{-2}$	$2.82 \times 10^{-2}$	$2.08 \times 10^{-2}$	$1.45 \times 10^{-2}$	$9.22 \times 10^{-3}$	$5.14 \times 10^{-3}$	$2.85 \times 10^{-11}$
200	$2.48 \times 10^{-2}$	$1.84 \times 10^{-2}$	$1.28 \times 10^{-2}$	$8.08 \times 10^{-3}$	$4.50 \times 10^{-3}$	$2.02 \times 10^{-3}$	$6.27 \times 10^{-4}$	$1.15 \times 10^{-4}$	$8.19 \times 10^{-6}$	$1.00 \times 10^{-6}$	$2.63 \times 10^{-13}$

Table II The light vector scenario production cross sections times branching ratios (in fb) at Leading Order (LO) for different choices of the DM mass  $M_{\chi_1}$  (in GeV) and  $Z'$  mass  $M_{Z'}$  (in GeV); for the light-dark sector mass assumption with the following couplings constants  $g_l = 0.003$ ,  $g_{DM} = 1.0$ . Given that the polarized degrees of electron and positron beams are  $P_{e^-} = 0.8$ ,  $P_{e^+} = -0.3$  at the ILC with  $\sqrt{s} = 500 \text{ GeV}$ .

The polarized degrees of electron and positron beams are  $P_{e^-} = 0.8$  and  $P_{e^+} = -0.3$ , respectively, at the ILC with  $\sqrt{s} = 500$  GeV.

The Monte Carlo simulations were used to generate the SM background samples and calculate their corresponding cross-sections for this analysis. The calculations were done in leading order and can be found in table III. The signal samples and SM background processes were estimated from these simulations and were normalized to their respective cross sections and an integrated luminosity of  $1000 \text{ fb}^{-1}$ .

An ad-hoc flat 10% uncertainty is applied to cover all possible systematic effects.

## V. EVENT SELECTION

The event selection process has been designed to reconstruct a final state consisting of two muons with low transverse momentum ( $p_T$ ) and missing transverse energy accounting for the dark matter candidate. The selection is made by applying cuts on various kinematic parameters.

Both muons must pass a preliminary selection that includes the following criteria:

- $p_T^\mu$  (GeV)  $> 10$ ,
- $|\eta^\mu|$  (rad)  $< 2.5$ ,
- IsolationVar  $< 0.1$ .

Here, "IsolationVar" represents the isolation cut in DELPHES software to reject muons produced inside jets. This cut requires that the scalar  $p_T$  sum of all muon tracks within a cone of  $\Delta R = 0.5$  around the muon candidate, excluding the muon candidate itself, should not exceed 10% of the  $p_T$  of the muon.

Each event is selected based on two opposite-charge muons, with the condition that the dimuon invariant mass  $M_{\mu^+\mu^-}$  is greater than 10 GeV.

Figure 2 shows the distribution of the dimuon invariant mass for events passing pre-selection listed in table IV; The cyan histogram represents the Drell-Yan background, the yellow histogram stands for the vector boson pair backgrounds (WW and ZZ), and the red histogram represents the  $t\bar{t}$  background. These histograms are stacked. While the signals of the LV scenario, which have been generated with different masses (50 and 100 GeV) of the  $Z'$  boson and fixing the dark matter mass ( $M_{\chi_1} = 1$  GeV), are represented by different colored lines, and are overlaid.

We present the  $\cos\theta_{CS}$  distribution for a resonant model based on the light vector scenario in Figure 3. The model assumes a dark boson ( $Z'$ ) mass of 20 GeV, and we compare it with the irreducible backgrounds WW and ZZ( $2\mu 2\nu$ ) events. All events meet the pre-selection criteria outlined in Table IV and have a reconstructed invariant mass ranging from 18 to 45 GeV. The results are illustrated with a dotted line representing the model signal and blue and green lines for the WW and ZZ events, normalized to unity. We observe a clear distinction be-

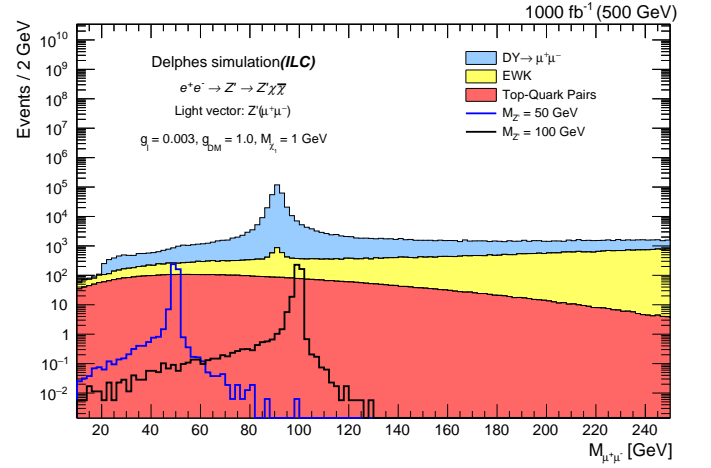


Figure 2 The measured dimuon invariant mass spectrum, after applying pre-selection summarized in table IV, for the estimated SM backgrounds and different choices of neutral gauge boson ( $Z'$ ) masses generated based on the LV scenario, with dark matter mass ( $M_{\chi_1} = 1$  GeV).

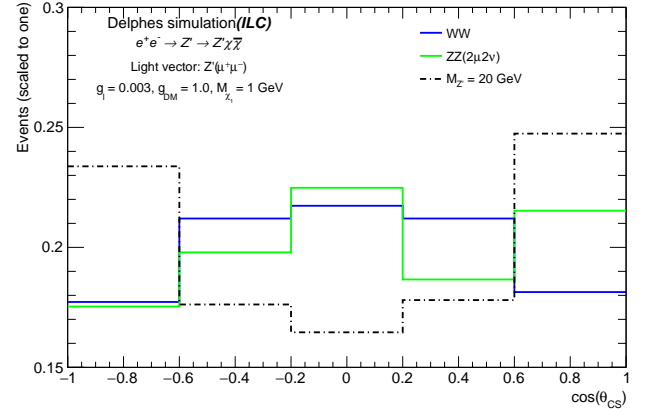


Figure 3 Normalized distributions of  $\cos\theta_{CS}$  for one resonant model based on LV scenario generated with a mass of  $Z'$  equal to 20 GeV, WW, and ZZ( $2\mu 2\nu$ ) events at  $\sqrt{s} = 500$  GeV. All events must pass the pre-selection listed in table IV and have a reconstructed invariant mass in the 18 - 45 GeV range. All histograms are normalized to unity to highlight qualitative features.

tween the simplified model and the WW and ZZ events. The signal shape exhibits a typical characteristic of a spin-1 boson, displaying a symmetric distribution around zero. This distribution aligns with the findings from the study conducted in [48].

The distributions of  $\cos\theta_{CS}$  are illustrated in Figure 4 for events that meet the pre-selection criteria outlined in Table IV. The histograms depict the expected outcomes from the standard model, alongside signal samples from the light vector model for different mass val-



Process	Decay channel	Generator	$\sigma \times \text{BR}$ (fb)	Order
DY	$\mu^+\mu^-$	Whizard	1767	LO
t $\bar{t}$	$\mu^+\mu^- + 2b + 2\nu$	Whizard	10.4	LO
WW	$\mu^+\mu^- + 2\nu$	Whizard	232.8	LO
ZZ	$\mu^+\mu^- + 2\nu$	Whizard	3.7	LO
ZZ	$4\mu$	Whizard	0.5	LO

Table III The simulated SM backgrounds generated from electron-positron collisions at the ILC with the polarized degrees of electron and positron beams are  $P_{e^-} = 0.8$ ,  $P_{e^+} = -0.3$  at  $\sqrt{s} = 500$  GeV. Their corresponding cross-section times branching ratio for each process and the generation order are presented. Names of these MC samples and the used generators are stated as well.

ues  $M_{A'}$  ranging from 20 to 60 GeV. This analysis zeroes in on various dimuon mass windows, specifically:  $18 < M_{\mu^+\mu^-} < 45$  GeV 4(a),  $27 < M_{\mu^+\mu^-} < 55$  GeV 4(b),  $36 < M_{\mu^+\mu^-} < 65$  GeV 4(c),  $45 < M_{\mu^+\mu^-} < 75$  GeV 4(d),  $54 < M_{\mu^+\mu^-} < 85$  GeV 4(e). The plots indicate that the signal samples are heavily contaminated by background events across the entire dimuon invariant mass range. Consequently, as will be discussed in the next paragraph, it is essential to implement stricter criteria to effectively distinguish the signals from Standard Model backgrounds.

In addition to the pre-selection criteria, we have applied tighter cuts based on six variables:

1. **\*\*Invariant Mass of the Dimuon\*\***: We restrict the invariant mass of the dimuon to a narrow range around the mass of the neutral gauge boson  $Z'$ . Specifically, we require that  $0.9 \times M_{Z'} < M_{\mu^+\mu^-} < M_{Z'} + 25$ , as suggested in reference [36].

2. **\*\*Relative Momentum Difference\*\***: We assess the relative difference between the momentum of the dimuon ( $p^{\mu^+\mu^-}$ ) and the missing transverse energy ( $E_T^{\text{miss}}$ ). This difference is selected to be less than 0.1, defined by the condition  $|p^{\mu^+\mu^-} - E_T^{\text{miss}}|/p^{\mu^+\mu^-} < 0.1$ .

3. **\*\*Azimuthal Angle Difference\*\***: We calculate the azimuthal angle difference  $\Delta\phi_{\mu^+\mu^-, \vec{E}_T^{\text{miss}}}$ , which is the difference between the azimuthal angles of the dimuon and the missing transverse energy ( $|\phi^{\mu^+\mu^-} - \phi^{\text{miss}}|$ ). This value is required to be greater than 3.0 radians.

4. **\*\*Angular Separation Between Muons\*\***: We examine the angular separation  $\Delta R(\mu^+\mu^-)$  between the two opposite-sign muons, which must be less than 1.4.

5. **\*\*3D Angle\*\***: We apply a criterion on the cosine of the 3D angle between the missing energy vector and the dimuon system vector to ensure they are back-to-back, requiring that  $\cos(\text{Angle}_{3D}) < -0.9$ .

6. Finally, we impose a cut on the missing transverse energy, requiring that  $E_T^{\text{miss}} > 100$  GeV.

The graphs in Figure 5 illustrate the distributions of specific variables for two signal presentations ( $M_{Z'} = 20$  and 80 GeV) of the simplified model related to the light vector scenario. These variables are shown alongside the Standard Model (SM) backgrounds for dimuon events that pass the pre-selection listed in table IV.

The first variable is represented as  $|p^{\mu^+\mu^-} -$

$E_T^{\text{miss}}|/p^{\mu^+\mu^-}$ , and its graph is displayed in Plot 5(a). The second variable is denoted as  $\Delta\phi_{\mu^+\mu^-, \vec{E}_T^{\text{miss}}}$ , with its corresponding graph shown in Plot 5(b). The third variable measures the angular distance between the two muons and is referred to as  $\Delta R(\mu^+\mu^-)$ , which is presented in Plot 5(c). The fourth variable,  $\cos(\text{Angle}_{3D})$ , is illustrated in Plot 5(d). Finally, the fifth variable, the missing transverse energy  $E_T^{\text{miss}}$ , is presented in Plot 5(e). The plots presented here depict the Standard Model (SM) backgrounds and signals from the LV scenario. These signals are generated with a neutral gauge boson mass of  $M_{Z'} = 20$  GeV and 80 GeV, while the dark matter mass is set at  $M_{\chi_1} = 1$  GeV. The vertical black dashed lines in these plots indicate the selected cut values for each variable.

Figure 6 shows the dimuon invariant mass spectrum for events that meet the semi-final selection criteria listed in Table IV. The histograms represent the estimated SM backgrounds and various light neutral gauge boson ( $Z'$ ) masses ( $M_{Z'} = 50$  and 100 GeV) generated based on the LV simplified model, with a dark matter mass of  $M_{\chi_1} = 1$  GeV.

Based on the semi-final selection analysis previously discussed, the Standard Model (SM) background is notably diminished. Additionally, the Drell-Yan background is eliminated. As a result, signal events are distinguishable from the SM background.

## VI. RESULTS

The shape-based analysis utilizes the distributions of  $\cos(\theta_{CS})$  as effective discriminators. These distributions are particularly useful because the signal characteristic is defined by a typical spin-1 boson pattern, which notably differs from that of the Standard Model backgrounds. After applying the final event selection listed in table IV, the  $\cos(\theta_{CS})$  distribution is illustrated in figure 7. This plot displays the results of both the SM backgrounds and the signal of the simplified LV scenario. The signal was generated with masses of a light gauge boson  $M_{Z'}$  of 20 GeV, and a dark matter mass  $M_{\chi_1}$  of 1 GeV, corresponding to an integrated luminosity of  $1000 \text{ fb}^{-1}$ .

To determine the required values of  $M_{Z'}$  necessary for observing either a deviation or a potential discov-

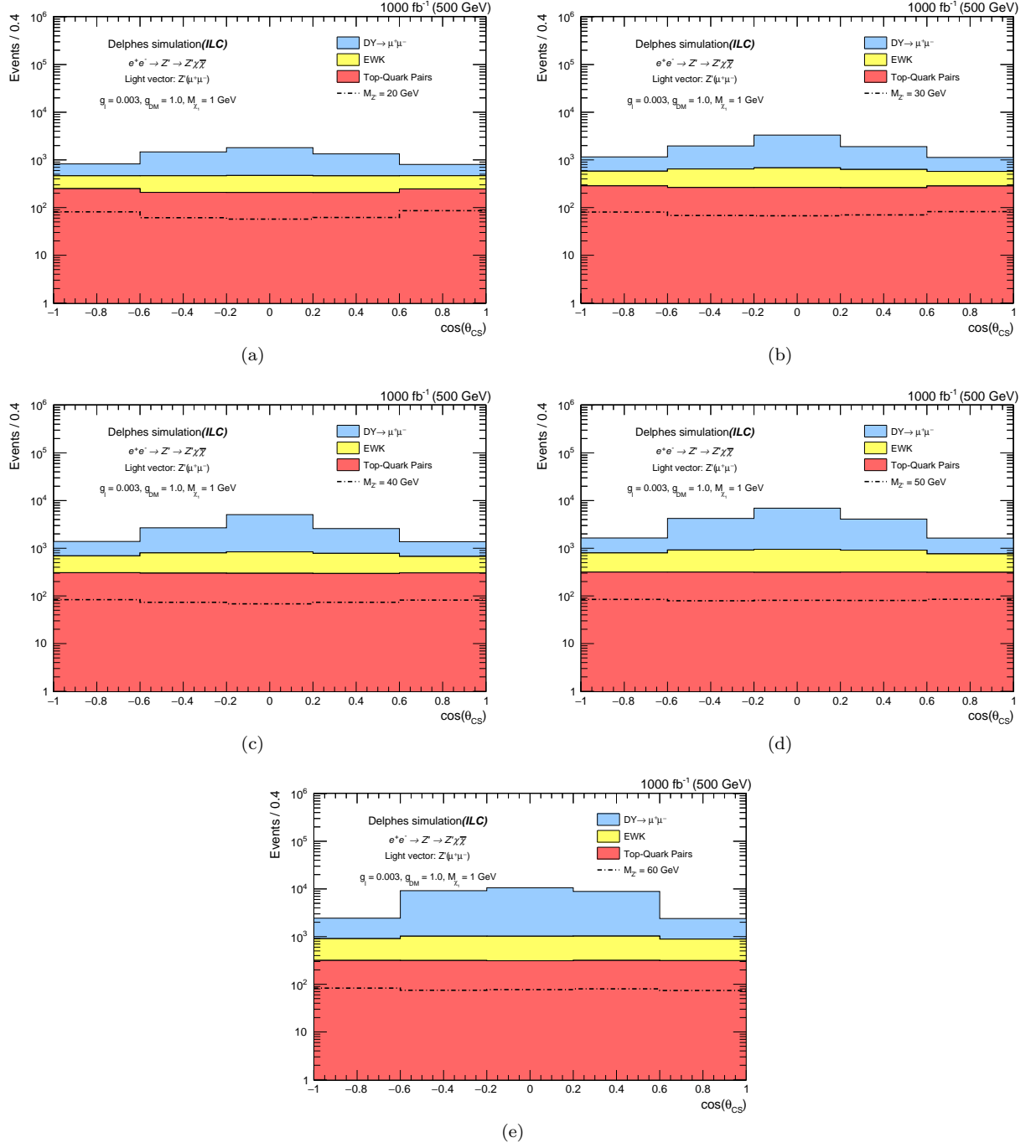


Figure 4 The distributions of  $\cos\theta_{CS}$  are presented for events that pass the pre-selection criteria listed in Table IV. The histograms show the standard model expectations, while the signal samples corresponding to the light vector model with different mass values  $M_{A'}$  ranging from 20 to 60 GeV are also superimposed. The analysis focuses on several dimuon mass windows, specifically:  $18 < M_{\mu^+\mu^-} < 45$  GeV 4(a),  $27 < M_{\mu^+\mu^-} < 55$  GeV 4(b),  $36 < M_{\mu^+\mu^-} < 65$  GeV 4(c),  $45 < M_{\mu^+\mu^-} < 75$  GeV 4(d),  $54 < M_{\mu^+\mu^-} < 85$  GeV 4(e).

ery, we have assessed the signal significance, defined as  $S = N_s / \sqrt{N_s + N_b}$ , by varying  $M_{Z'}$ . In this formula,  $N_s$  represents the number of signal events, while  $N_b$  denotes the total number of Standard Model background events that pass the final selection criteria outlined in Table IV.

Figure 8(a) shows the relationship between signal significance and  $M_{Z'}$  for various dark matter masses ( $M_{\chi_1}$ ). In contrast, Figures 8(b) and 8(c) illustrate the significance ( $S$ ) as a function of integrated luminosity for two scenarios of dark matter mass ( $M_{\chi_1} = 1$  GeV and 100

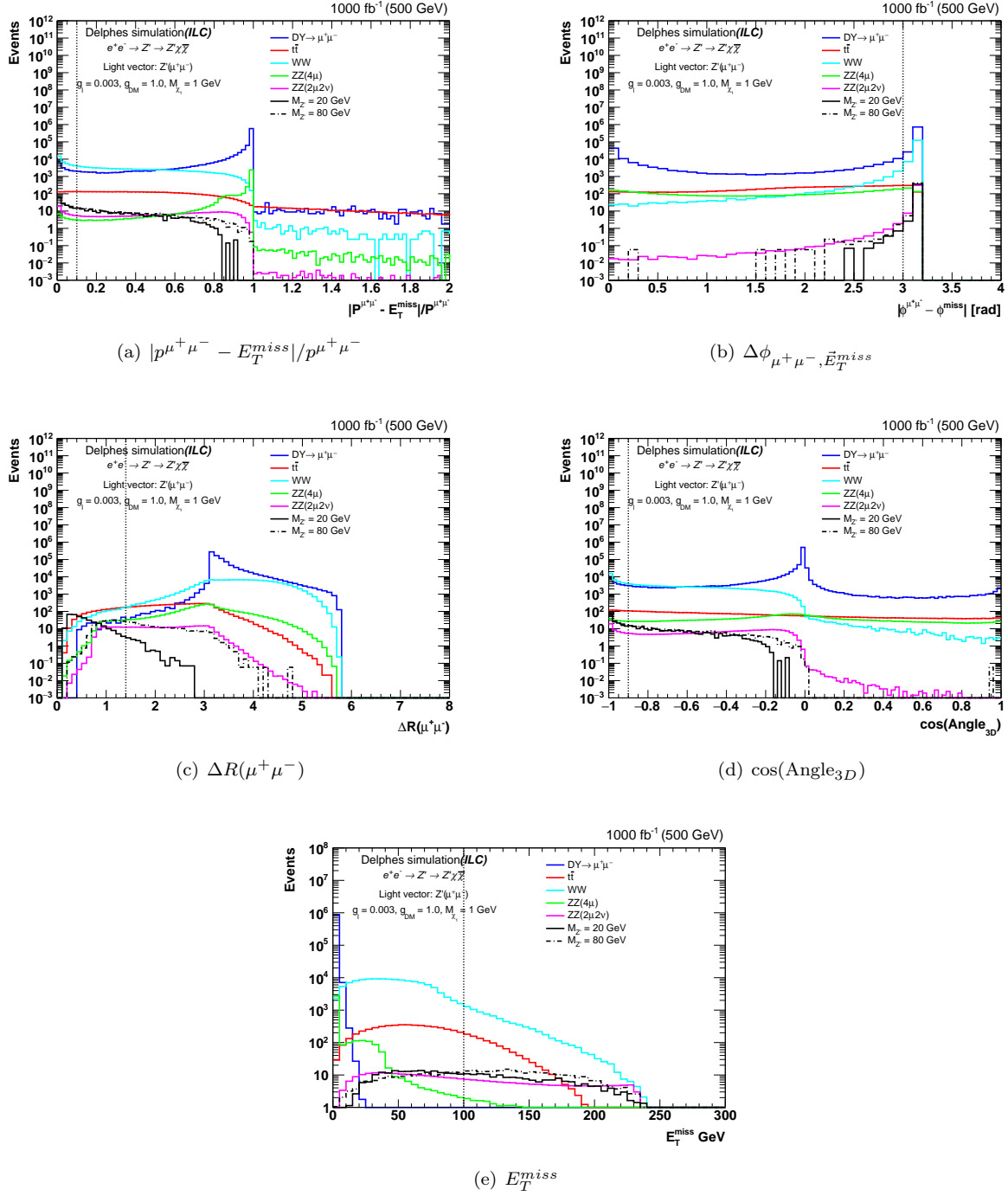


Figure 5 The distributions of restricted variables for dimuon events, where both muons satisfy the low  $p_T$  muon ID criteria discussed in the pre-selection in table IV. The five variables are  $|p^{\mu^+\mu^-} - E_T^{miss}|/p^{\mu^+\mu^-}$  5(a),  $\Delta\phi_{\mu^+\mu^-, \vec{E}_T^{miss}}$  5(b),  $\Delta R(\mu^+\mu^-)$  5(c),  $\cos(\text{Angle}_{3D})$  5(d), and the missing transverse energy  $E_T^{miss}$ , is presented in 5(e). The model corresponds to the LV scenario with two different values of  $Z'$  ( $M_{Z'} = 20$  and  $80$  GeV) and SM backgrounds. The vertical dashed lines correspond to the chosen cut value for each variable.

Pre-selection	Semi-final selection	Final selection
$p_T^\mu > 10 \text{ GeV}$ $ \eta^\mu  < 2.5 \text{ rad}$ $\Sigma_i p_T^i / p_T^\mu < 0.1$ $M_{\mu^+\mu^-} > 10 \text{ GeV}$	$p_T^\mu > 10 \text{ GeV}$ $ \eta^\mu  < 2.5 \text{ rad}$ $\Sigma_i p_T^i / p_T^\mu < 0.1$ $M_{\mu^+\mu^-} > 10 \text{ GeV}$ $ p^{\mu^+\mu^-} - E_T^{\text{miss}}  / p^{\mu^+\mu^-} < 0.1$ $\Delta\phi_{\mu^+\mu^-, \vec{E}_T^{\text{miss}}} > 3 \text{ rad}$ $\Delta R(\mu^+\mu^-) < 1.4$ $\cos(\text{Angle}_{3D}) < -0.9$ $E_T^{\text{miss}} > 100 \text{ GeV}$	$p_T^\mu > 10 \text{ GeV}$ $ \eta^\mu  < 2.5 \text{ rad}$ $\Sigma_i p_T^i / p_T^\mu < 0.1$ $0.9 \times M_{Z'} < M_{\mu^+\mu^-} < M_{Z'} + 25$ $ p^{\mu^+\mu^-} - E_T^{\text{miss}}  / p^{\mu^+\mu^-} < 0.1$ $\Delta\phi_{\mu^+\mu^-, \vec{E}_T^{\text{miss}}} > 3 \text{ rad}$ $\Delta R(\mu^+\mu^-) < 1.4$ $\cos(\text{Angle}_{3D}) < -0.9$ $E_T^{\text{miss}} > 100 \text{ GeV}$

Table IV Summary of cut-based event selections used in the analysis.

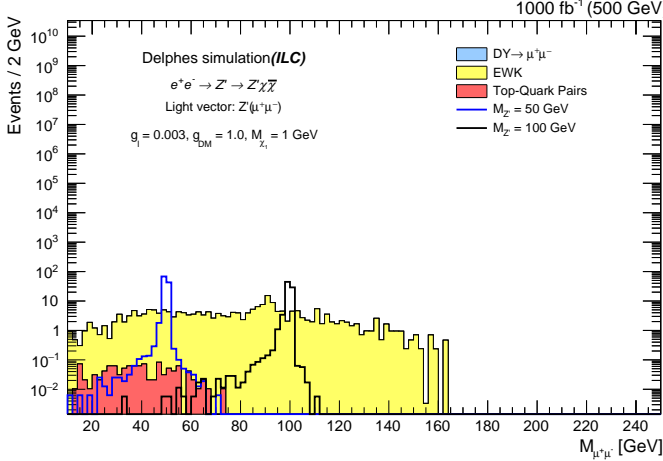


Figure 6 The dimuon invariant mass spectrum, for events passing the semi-final selection listed in table IV, for the estimated SM backgrounds and different choices of light gauge boson ( $Z'$ ) masses generated based on the LV simplified model, with dark matter mass ( $M_{\chi_1} = 1 \text{ GeV}$ ).

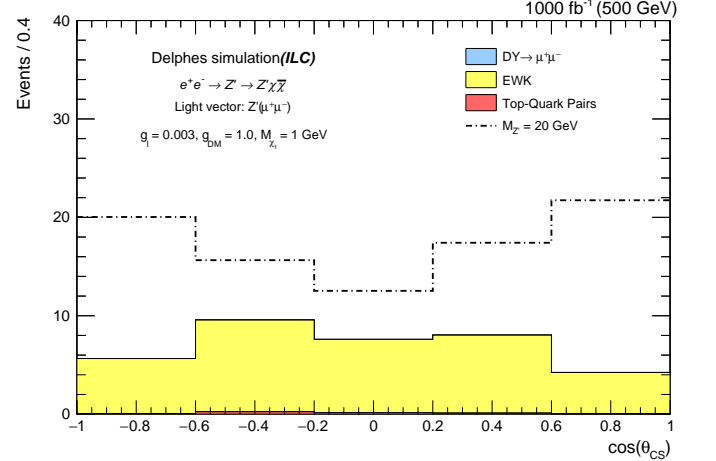


Figure 7 The distribution of the  $\cos(\theta_{CS})$ , after applying the final analysis listed in table IV, for the expected SM background and one signal benchmark corresponding to the LV with  $M_{Z'} = 20 \text{ GeV}$  is superimposed. All events are required to have an invariant mass of the dimuon in the range of 18 to 45 GeV.

GeV). Figure 8(b) focuses on  $M_{Z'} = 50 \text{ GeV}$ , while Figure 8(c) focuses on  $M_{Z'} = 100 \text{ GeV}$ , for events that meet final criteria outlined in Table IV. These figures reflect the model associated with the LV scenario, using coupling constants of  $g_l = 0.003$  and  $g_{DM} = 1.0$ . Additionally, the polarization degrees of the electron and positron beams at the ILC are set at  $P_{e^-} = 0.8$  and  $P_{e^+} = -0.3$ . The dashed red line in the plots signifies a significance value of  $S = 5$ .

For  $M_{Z'} = 50 \text{ GeV}$ , one can achieve a  $5\sigma$  discovery at an integrated luminosity of  $365 \text{ fb}^{-1}$  for low mass dark matter ( $M_{\chi_1} = 1$ ) GeV, while requiring  $1190 \text{ fb}^{-1}$  for heavy dark matter ( $M_{\chi_1} = 100$ ) GeV.

For a  $M_{Z'}$  of  $100 \text{ GeV}$ , a  $5\sigma$  discovery can be achieved at an integrated luminosity of  $600 \text{ fb}^{-1}$  for low-mass dark matter with a mass  $M_{\chi_1} = 1 \text{ GeV}$ . However, for heavy dark matter with a mass  $M_{\chi_1} = 100 \text{ GeV}$ , it is not possible to achieve a  $5\sigma$  discovery even with the total integrated luminosity available at the ILC.

We used the profile likelihood method to analyze our

results statistically and performed a statistical test based on the  $\cos(\theta_{CS})$  distributions. We used the modified frequentist construction CLs [49, 50], which is based on the asymptotic approximation [51], to derive exclusion limits on the product of signal cross sections and the branching fraction  $\text{Br}(Z' \rightarrow \mu\mu)$  at a 95% confidence level.

In the mono- $Z'$  model, the 95% upper limit on the cross-section times the branching ratio for the LV simplified scenario is shown in Figure 9. The result is presented for the muonic decay of the  $Z'$  and with coupling constant values of  $g_l = 0.003$  and  $g_{DM} = 1.0$ , for an integrated luminosity of  $1000 \text{ fb}^{-1}$ . The limits are depicted for dark matter mass values of  $M_{\chi_1}$  at 1, 100, 125, 130, 140, 150, and 160 GeV, each represented by a distinct colored solid line.

Figure 10 shows the limit on the cross-sections times the branching ratios for the muonic decay channel of the  $Z'$  boson as functions of the mediator's mass ( $M_{Z'}$ ) and the mass of the dark matter ( $M_{\chi_1}$ ). The region inside the contour is excluded for the benchmark scenario where



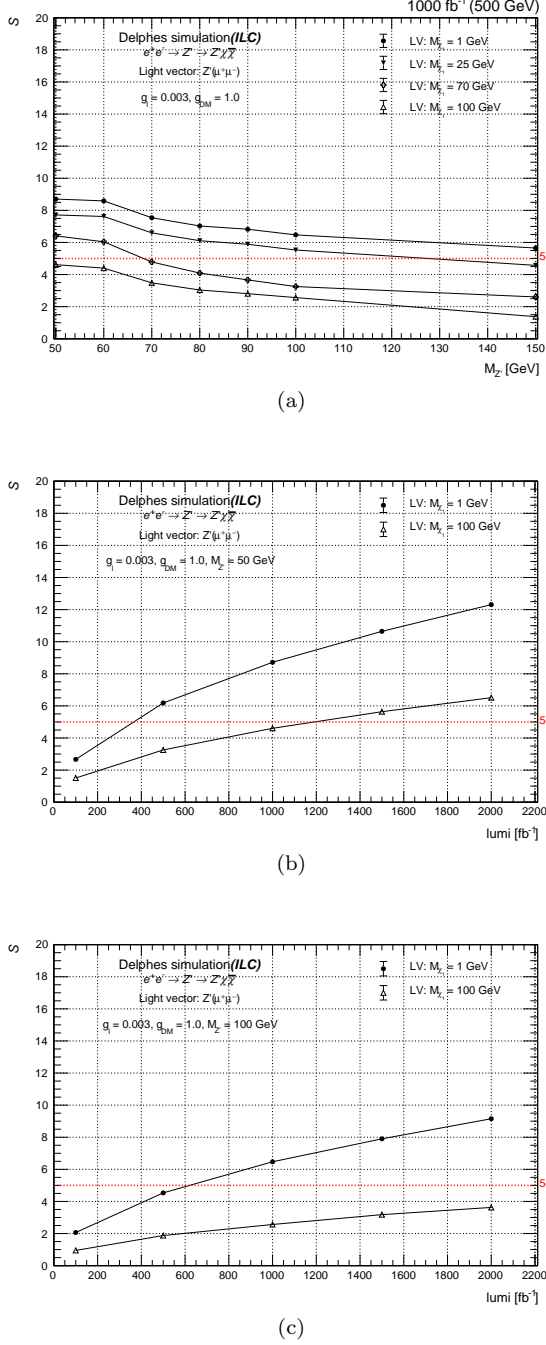


Figure 8 The significance ( $S$ ) versus  $M_{Z'}$  in 8(a), and Integrated luminosity in 8(b) and 8(c) plotted at different dark matter masses ( $M_{\chi_1}$ ) for events passing the full set of cuts listed in table IV. The model corresponds to the LV scenario with the coupling constants  $g_l = 0.003$ ,  $g_{DM} = 1.0$ . Given that the polarized degrees of electron and positron beams are  $P_{e^-} = 0.8$ ,  $P_{e^+} = -0.3$  at the ILC. The dashed horizontal red line corresponds to  $S = 5$ .

$g_l = 0.003$  and  $g_{DM} = 1.0$ . We used an integrated luminosity of  $1000 \text{ fb}^{-1}$ . This limit shows that the invariant mass range from 20 to 100 GeV can be excluded for  $M_{\chi_1} \in [1, 100] \text{ GeV}$ .

## VII. SUMMARY

The International Linear Collider (ILC) electron-positron collider is an ideal machine for discovering particles that lie beyond the Standard Model (BSM). It provides a clear signature for identifying unknown particles such as dark matter, extra neutral gauge bosons, and Kaluza-Klein excitations, all against a background of quantum chromodynamics (QCD).

Our research investigated the angular distributions of low-mass dimuon pairs within the Collins-Soper frame, using simulated data samples from the ILC. These Monte Carlo (MC) samples were generated from electron-positron collisions with a center-of-mass energy of 500 GeV, including signal and Standard Model background events. This setup corresponds to what is anticipated for ILC Run 1, which is expected to have an integrated luminosity of  $1000 \text{ fb}^{-1}$ . Our analysis focused on the  $\cos\theta_{CS}$  variable to extract valuable insights from the MC data.

In this study, we investigated the effects of a simplified model scenario known as the light vector (LV), focusing on dark matter pair production associated with a  $Z'$  boson at the ILC. We analyzed the results from the muonic decay mode of the  $Z'$  boson, with coupling constants fixed at  $g_{DM} = 1.0$  and  $g_l = 0.003$ . Furthermore, the polarization levels of the electron and positron beams were set at  $P_{e^-} = 0.8$  and  $P_{e^+} = -0.3$ , respectively, for this analysis.

We implemented effective discrimination cuts that successfully eliminated the Drell-Yan (DY) background, allowing us to better differentiate between signal events and Standard Model (SM) backgrounds. As a result, we observed a significant reduction in SM backgrounds while preserving the signal strength by applying appropriate cuts, which are detailed in Table IV for the light vector scenario.

With the strong cuts applied, a mass  $M_{Z'}$  of 50 GeV allows us to achieve a  $5\sigma$  discovery at an integrated luminosity of  $365 \text{ fb}^{-1}$  for low-mass dark matter ( $M_{\chi_1} = 1 \text{ GeV}$ ). In comparison, obtaining this for heavy dark matter ( $M_{\chi_1} = 100 \text{ GeV}$ ) requires an integrated luminosity of  $1190 \text{ fb}^{-1}$ .

While for a  $M_{Z'}$  of 100 GeV, a  $5\sigma$  discovery can be achieved at an integrated luminosity of  $600 \text{ fb}^{-1}$  for low-mass dark matter ( $M_{\chi_1} = 1 \text{ GeV}$ ). However, for heavy dark matter with a mass of  $M_{\chi_1} = 100 \text{ GeV}$ , it is not possible to achieve a  $5\sigma$  discovery, even with the total integrated luminosity available at the ILC.

If this signal is not observed at the ILC, we set upper limits on the masses of  $Z'$  and dark matter ( $\chi_1$ ) at the 95% confidence level for the charged muonic decay channel of  $Z'$ .

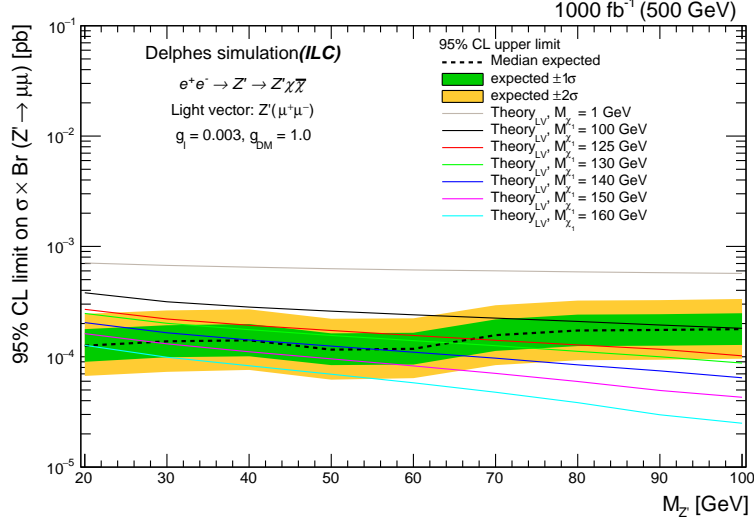


Figure 9 95% CL upper limits on the cross-section times the branching ratio (expected), as a function of the mediator's mass ( $M_{Z'}$ ) based on mono- $Z'$  model, with the muonic decay of the  $Z'$ . The solid colored lines represent the light vector scenario with  $M_{\chi_1} = 1, 100, 125, 130, 140, 150,$  and  $160$  GeV.

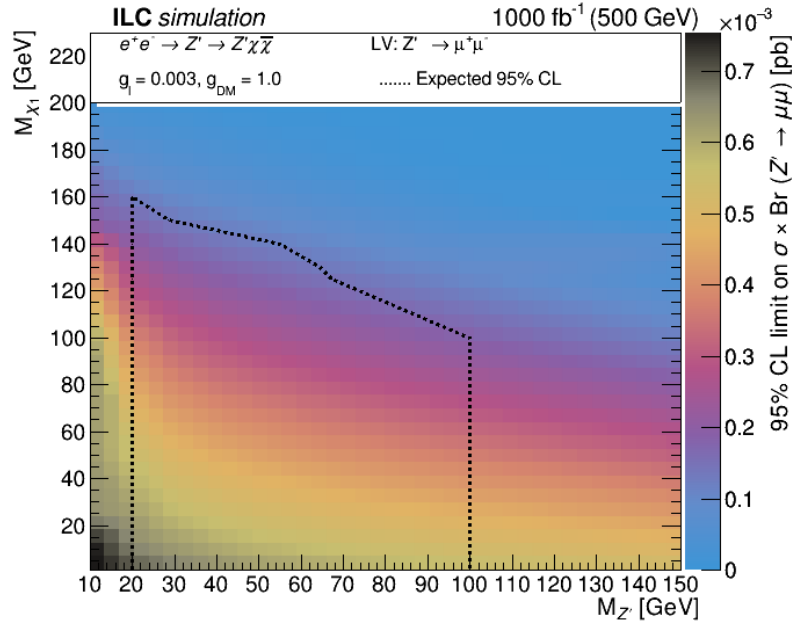


Figure 10 The 95% CL upper limits on the product of the cross-section times branching ratio from the inclusive search, for variations of pairs of the LV scenario parameters ( $M_{Z'}$  and  $M_{\chi_1}$ ). The filled region indicates the upper limit. The dotted black curve indicates the expected exclusions for the nominal  $Z'$  cross-section.

Limits have been established for the light vector scenario with  $g_l = 0.003$  and  $g_{DM} = 1.0$ , which excludes the invariant mass range from 20 to 100 GeV for  $M_{\chi_1}$  in the range of 1 to 100 GeV. However, it does exclude  $M_{\chi_1} = 160$  GeV when  $M_{Z'} = 20$  GeV.

Additionally, for high dark matter mass values (i.e.,  $M_{\chi_1} > 160$  GeV), the ILC will be insensitive to the light

vector scenario.

## ACKNOWLEDGMENTS

The author of this paper would like to thank Tongyan Lin, co-author of [36], for providing us with the UFO

model files, helping us to generate the signal events, and cross-checking the results. In addition, this paper is

based on works supported by the Science, Technology, and Innovation Funding Authority (STIF) under grant number 48289.

- 
- [1] P. Langacker, The Physics of Heavy  $Z'$  Gauge Bosons. *Rev. Mod. Phys.*, 81:1199–1228, 2008.
  - [2] L. Randall and R. Sundrum, A large mass hierarchy from a small extra dimension. *Phys. Rev. Lett.*, 83:3370–3373, 1999.
  - [3] Lane K. Eichten, E. and M. Peskin, New Tests for Quark and Lepton Substructure. *Phys. Rev. Lett.*, 50(11):811814, 1983.
  - [4] E. Eichten et al., Supercollider physics. *Rev. Mod. Phys.*, 56(4):579707, 1984.
  - [5] Dimopoulos S. Arkani Hamed, N. and G. Dvali, Phenomenology, Astrophysics and Cosmology of Theories with Sub-Millimeter Dimensions and TeV Scale Quantum Gravity. *Phys. Rev. D.*, 59(8), 1999.
  - [6] The CMS Collaboration, Search for resonant and nonresonant new phenomena in high mass dilepton final states at  $\sqrt{s} = 13$  TeV. *JHEP* 07 (2021) 208.
  - [7] M. Cvetič and S. Godfrey, “Discovery and identification of extra gauge bosons”, [arXiv:hep-ph/9504216](#).
  - [8] A. Leike, “The Phenomenology of extra neutral gauge bosons”, *Phys. Rep.* 317, 143 (1999) [[arXiv:hep-ph/9805494](#)].
  - [9] M. Cvetič, P. Langacker, and B. Kayser, “Determination of g-R / g-L in left-right symmetric models at hadron colliders”, *Phys. Rev. Lett.* 68 (1992) 2871.
  - [10] S. Dimopoulos and H. Georgi, “Softly Broken Supersymmetry And  $SU(5)$ ”, *Nucl. Phys. B* 193 (1981) 150.
  - [11] ATLAS Collaboration, Search for high-mass dilepton resonances using 139 fb $^{-1}$  of  $pp$  collision data collected at  $\sqrt{s} = 13$  TeV with the ATLAS detector, *Phys. Lett. B* 796 (2019) 68.
  - [12] CMS Collaboration, Forward-backward asymmetry of Drell-Yan lepton pairs in  $pp$  collisions at  $\sqrt{s} = 8$  TeV. *Eur. Phys. J. C* 76 (2016) 325.
  - [13] ATLAS Collaboration, Measurement of the angular coefficients in Z-boson events using electron and muon pairs from data taken at  $\sqrt{s} = 8$  TeV with the ATLAS detector. *JHEP* 08 (2016) 159.
  - [14] CMS Collaboration, Measurement of the Drell-Yan forward-backward asymmetry at high dilepton masses in proton-proton collisions at  $\sqrt{s} = 13$  TeV. *JHEP* 08 (2022) 063.
  - [15] CMS Collaboration, Dark sector searches with the CMS experiment. *Phys. Rept.* 1115 (2025) 448.
  - [16] ATLAS Collaboration, Exploration at the high-energy frontier: ATLAS Run 2 searches investigating the exotic jungle beyond the Standard Model. *Phys. Rep.* 1116 (2025) 301-385.
  - [17] Krovi Anirudh, Low Ian and Zhang Yue, Broadening dark matter searches at the LHC: mono-X versus darkonium channels. *JHEP* 10 (2018) 026 [[arXiv:1807.07972](#)] [[hep-ph](#)].
  - [18] CMS Collaboration, Search for new physics in final states with an energetic jet or a hadronically decaying W or Z boson and transverse momentum imbalance at  $\sqrt{s} = 13$  TeV, *Phys. Rev. D* 97 (2018) 092005. [[arXiv:1712.02345](#)] [[hep-ex](#)].
  - [19] ATLAS Collaboration, Search for dark matter in events with a hadronically decaying vector boson and missing transverse momentum in  $pp$  collisions at  $\sqrt{s} = 13$  TeV with the ATLAS detector, *JHEP* 10 (2018) 180 [[arXiv:1807.11471](#)] [[hep-ex](#)].
  - [20] CMS Collaboration, Search for dark matter produced in association with a leptonically decaying Z boson in proton-proton collisions at  $\sqrt{s} = 13$  TeV. *Eur. Phys. J. C* 81 (2021) 13; Erratum: *Eur. Phys. J. C* 81 (2021) 333.
  - [21] ATLAS Collaboration, Search for associated production of a Z boson with an invisibly decaying Higgs boson or dark matter candidates at  $\sqrt{s} = 13$  TeV with the ATLAS detector. *Phys. Lett. B* 829 (2022) 137066.
  - [22] CMS Collaboration, Search for new physics in the monophoton final state in proton-proton collisions at  $\sqrt{s} = 13$  TeV, *JHEP*. 10 (2017) 073, [[arXiv:1706.03794v2](#)] [[hep-ex](#)].
  - [23] ATLAS Collaboration, Search for dark matter in association with an energetic photon in  $pp$  collisions at  $\sqrt{s} = 13$  TeV with the ATLAS detector, *JHEP* 02 (2021) 226, [[arXiv:2011.05259v2](#)] [[hep-ex](#)].
  - [24] CMS Collaboration, Search for dark matter particles produced in association with a Higgs boson in proton-proton collisions at  $\sqrt{s} = 13$  TeV, *JHEP* 03 (2020) 025, [[arXiv:1908.01713v2](#)] [[hep-ex](#)].
  - [25] ATLAS Collaboration, Search for dark matter produced in association with a Standard Model Higgs boson decaying into b-quarks using the full Run 2 dataset from the ATLAS detector, *JHEP* 11 (2021) 209, [[arXiv:2108.13391v2](#)] [[hep-ex](#)].
  - [26] ATLAS Collaboration, Search for dark matter in events with missing transverse momentum and a Higgs boson decaying into two photons in  $pp$  collisions at  $\sqrt{s} = 13$  TeV with the ATLAS detector, *JHEP* 10 (2021) 13, [[arXiv:2104.13240v2](#)] [[hep-ex](#)].
  - [27] Neng, W., Mao, S., Gang, L. et al. Searching for dark matter via mono-Z boson production at the ILC. *Eur. Phys. J. C* 74, 3219 (2014). <https://doi.org/10.1140/epjc/s10052-014-3219-2>.
  - [28] Dutta, S., Rawat, B., Sachdeva, D. Signals of leptophilic dark matter at the ILC. *Eur. Phys. J. C* 77, 639 (2017). <https://doi.org/10.1140/epjc/s10052-017-5188-8>.
  - [29] Kalinowski, J., Kotlarski, W., Mekala, K. et al. Sensitivity of future linear colliders to processes of dark matter production with light mediator exchange. *Eur. Phys. J. C* 81, 955 (2021). <https://doi.org/10.1140/epjc/s10052-021-09758-6>.
  - [30] Moritz Habermehl, Mikael Berggren, and Jenny List, WIMP dark matter at the International Linear Collider. *PHYSICAL REVIEW D* 101, 075053 (2020).
  - [31] Howard Baer, Tim Barklow, Keisuke Fujii, et al. The International Linear Collider Technical Design Report - Volume 2: Physics. ILC-REPORT-2013-040; ANL-HEP-TR-13-20; BNL-100603-2013-IR; IRFU-13-59; CERN-ATS-2013-037; Cockcroft-13-10; CLNS 13/2085; DESY

- 13-062; FERMILAB TM-2554; IHEP-AC-ILC-2013-001; INFN-13-04/LNF; JAI-2013-001; JINR E9-2013-35; JLAB-R-2013-01; KEK Report 2013-1; KNU/CHEP-ILC-2013-1; LLNL-TR-635539; SLAC-R-1004; ILC-HiGrade-Report-2013-003, [arXiv:1306.6352](#) [hep-ph].
- [32] CLIC, CLICdp collaborations, The Compact Linear Collider (CLIC) - 2018 Summary Report. CERN-2018-005-M, [arXiv:1812.06018](#) [physics.acc-ph].
- [33] ATLAS collaboration, Search for a new  $Z'$  gauge boson in  $4\mu$  events with the ATLAS experiment, JHEP 07 (2023) 90.
- [34] CMS collaboration, Search for an  $L_\mu-L_\tau$  gauge boson using  $Z \rightarrow 4\mu$  events in proton-proton collisions at  $\sqrt{s} = 13$  TeV, Phys. Lett. B 792 (2019) 345.
- [35] ATLAS Collaboration, Search for a new leptonically decaying neutral vector boson in association with missing transverse energy in proton-proton collisions at  $\sqrt{s} = 13$  TeV with the ATLAS detector, ATLAS-CONF-2023-045, 18 August 2023.
- [36] Marcelo Autran, Kevin Bauer, Tongyan Lin, and Daniel Whiteson, Searches for dark matter in events with a resonance and missing transverse energy. Physical Review D 92 (2015) 035007 [[arXiv:1504.01386](#)] [hep-ph].
- [37] A. Gupta, R. Primulando, P. Saraswat, A new probe of dark sector dynamics at the LHC. JHEP 09, 079 (2015). [[arXiv:1504.01385](#)] [hep-ex].
- [38] LEP et al. collaborations, A combination of preliminary electroweak measurements and constraints on the Standard Model, [hep-ex/0312023](#) [INSPIRE].
- [39] Arnab Dasgupta, P. S. Bhupal Dev, Tao Han, Rojalin Padhan, Si Wang, Keping Xie, Searching for heavy leptophilic  $Z'$ : from lepton colliders to gravitational waves, JHEP 12 (2023) 011.
- [40] J. Brau, Y. Okada, N. Walker, [arXiv:0712.1950](#) [physics.acc-ph].
- [41] A. Djouadi et al., [arXiv:0709.1893](#) [hep-ph]
- [42] N. Phinney, N. Toge, N. Walker, [arXiv:0712.2361](#) [physics.acc-ph]
- [43] T. Behnke et al., ArXiv e-prints (2007). [arXiv:0712.2356](#) [physics.ins-det]
- [44] J. Collins and D. Soper, Angular distribution of dileptons in high-energy hadron collisions. Phys. Rev. D., 16(7):2219–2225, 1977.
- [45] Wolfgang Kilian, Thorsten Ohl, and Jurgen Reuter. WHIZARD—simulating multi-particle processes at LHC and ILC. The European Physical Journal C, 71(9), Sep 2011.
- [46] T. Sjostrand, S. Mrenna and P. Skands, PYTHIA 6.4 Physics and Manual [[arXiv:hep-ph/0603175](#)].
- [47] J. de Favereau, C. Delaere, P. Demin, A. Giammanco, V. Lemaitre, A. Mertens, M. Selvaggi, DELPHES 3, A modular framework for fast simulation of a generic collider experiment, JHEP 1402 (2014).
- [48] P. Osland, A. A. Pankov, A. V. Tsytrinov and N. Paver, Spin identification of the Randall-Sundrum resonance in lepton-pair production at the CERN LHC, PHYSICAL REVIEW D 78, 035008 (2008).
- [49] A. L. Read, Presentation of search results: the CLs technique, J. Phys. G: Nucl. Part. Phys. 28 (2002) 2693, doi:10.1088/0954-3899/28/10/313.
- [50] T. Junk, Confidence level computation for combining searches with small statistics, Nuclear Instruments and Methods in Physics Research Section A: Accelerators, Spectrometers, Detectors and Associated Equipment, Volume 434, Issues 2–3, 1999, Pages 435–443, ISSN 0168-9002, [https://doi.org/10.1016/S0168-9002\(99\)00498-2](https://doi.org/10.1016/S0168-9002(99)00498-2).
- [51] G. Cowan et al., Asymptotic formulae for likelihood-based tests of new physics, Eur. Phys. J. C 71 (2011), p. 1554, doi: 10.1140/epjc/s10052-011-1554-0, arXiv: 1007.1727 [physics.data-an], Erratum: Eur. Phys. J. C 73 (2013) 2501.